Incommensurability Effects on Dipolar Bosons in Optical Lattices

J Low Temp Phys (2016) 182:153–161
DOI 10.1007/s10909-015-1417-4

Incommensurability Effects on Dipolar Bosons in Optical Lattices

Fabio Cinti[1,2]

Received: 5 October 2015 / Accepted: 6 December 2015 / Published online: 29 December 2015

Abstract We present a study that investigated a quantum dipolar gas in continuous space where a potential lattice was imposed. Employing exact quantum Monte Carlo techniques, we analysed the ground-state properties of the scrutinised system, varying the lattice depth and the dipolar interaction. For system densities corresponding to a commensurate filling with respect to the optical lattice, we observed a simple crystal-to-superfluid quantum phase transition, being consistent with the physics of dipolar bosons in continuous space. In contrast, an incommensurate density showed the presence of a supersolid phase. Indeed, such a result opens up the tempting opportunity to observe a defect-induced supersolidity with dipolar gases in combination with a tunable optical lattice. Finally, the stability of the condensate was analysed at finite temperature.

Keywords Dipolar bosons · Lattice potentials · Supersolidity · Path integral quantum Monte Carlo

1 Introduction

During the last few years, tremendous development in the ability to control ultra-cold gases, characterised by long-ranged dipolar interactions, confined in optical lattices [1,2] has taken place. In particular, surprising results have been achieved in quantum gases composed of Rydberg atoms [3], polar molecules [4] or lanthanides such as erbium (Er) [5].

✉ Fabio Cinti
cinti@sun.ac.za

1 National Institute for Theoretical Physics (NITheP), Stellenbosch 7600, South Africa

2 Institute of Theoretical Physics, Stellenbosch University, Stellenbosch 7600, South Africa

From a theoretical perspective, long-range magnetic or electric dipolar interactions are considered as chief candidates for observing and controlling novel phases in quantum many-body systems [6,7]. One of these phases is known as supersolidity, featuring both diagonal and off-diagonal order [8]. As is well known, the interaction among defects is a key ingredient for driving such an intriguing phase. Although in a quantum regime the defect interaction is still a problem not entirely understood in detail, it appears well established as, in some cases, supersolidity yields as a result of defects delocalisation [9]. Considering a classical regime only, some authors have emphasised that the effective defect interactions in a self-assembled crystal can be tuned from attractive to repulsive using an external periodic superlattice [10].

Concerning a quantum regime, recent studies have pointed out that the supersolid phase can be observed in optical lattices [8,11–13]. For example, Pollet et al. [13] have studied a complete phase diagram of a two-dimensional system composed of cold polar molecules on a triangular lattice. The authors proposed a phase diagram that featured a crystal, a superfluid, and, more important, a supersolid phase. However, even if these studies have improved knowledge of the concept of supersolidity remarkably, they still remain focused on single-band lattice models. Quantum phases using approximations that take into account higher bands still remain a subject to be understood in full [14–16].

In this paper, we present the results concerning a boson dipolar system in continuous space where a potential lattice is imposed, in other words removing the usual tight-binding condition [16]. In such a continuous limit, the band structure is not completely formed, roughly depending on the potential depth.

Using exact quantum Monte Carlo methods, we studied the many-body system investigating different lattice depths and dipolar interaction strengths, considering a filling factor around $n = 1/3$. We showed that the behaviour of the dipolar systems in shallow lattices changed drastically considering a commensurate and an incommensurate filling of the lattice potential. In the first case, one can observe a simple superfluid-to-crystal quantum phase transition, as already discussed in Refs. [17,18]. Concerning the second situation, incommensurability features a defect-induced supersolidity, as originally proposed in Ref. [19].

The article is organised as follows: in the Sect. 2, we present the model Hamiltonian and the quantum Monte Carlo methods applied. The results are presented and discussed in Sect. 3. In particular, Sect. 3.1 refers to the ground-state configuration, while Sect. 3.2 is devoted to a regime of finite temperature. Finally, in Sect. 4, a number of conclusions are presented.

2 Model Hamiltonian and Methodology

We considered an ensemble of bosons interacting via a dipole-dipole potential confined in a two-dimensional optical lattice. The system is described by a quantum-mechanical many-body Hamiltonian as follows:

$$\mathcal{H} = \frac{\hbar^2}{2m}\sum_i \nabla_i^2 + \sum_{i<j}\frac{D}{r_{ij}^3} - \sum_i u_i(\mathbf{r}), \tag{1}$$

where m is the mass of a single particle, while $r_{ij} = |\mathbf{r}_i - \mathbf{r}_j|$ is the distance between particles i and j. D represents the characteristic strength of the interaction between two dipoles. The last term of the Hamiltonian refers to an optical triangular lattice potential

$$u(\mathbf{r}) = u_0 \left[\sin^2\left(\frac{x+\sqrt{3}y}{2r_0}\right) + \sin^2\left(\frac{-x+\sqrt{3}y}{2r_0}\right) + \sin^2\left(\frac{x}{r_0}\right)\right] \tag{2}$$

with u_0 being the lattice depth and r_0 the optical lattice constant. For the sake of clarity, we defined distances and energies in units of $d = D/r_0^3$.

As mentioned before, the model proposed in Eq. (1) was investigated using a quantum Monte Carlo technique [20]. More precisely, we sampled the density matrix of the system employing a path integral representation in continuous space. Our code was based on the well-known worm algorithm [21]. This methodology has been implemented in order to properly sample both configurations connected to the partition function and configurations related to the one-particle Matsubara Green function. Over the last decade, this technique has been successfully implemented for studying the quantum properties of different bosonic systems [22]. An all-inclusive discussion of this methodology is provided in Ref. [23]. Moreover, as pointed out lately [24], the employment of repulsive dipolar interactions combined with trapping potentials does not involve any particular pathology throughout the sampling stage.

The worm algorithm efficiently furnishes a numerically *exact* estimation of the statistical observables, such as, for instance, energy per particle, density distributions and superfluid fraction. In the following sections, we are going to pay particular attention to the last two quantities. Concerning the study of density distributions in a continuous system described by the Hamiltonian (1), we introduce the density profile as

$$n_1(\mathbf{r}) = \left\langle \sum_i \delta\left(\mathbf{r} - \mathbf{r}_i(t)\right) \right\rangle_t \tag{3}$$

$\langle \ldots \rangle_t$ denotes an average of the corresponding imaginary time trajectories $\mathbf{r}_i(t)$. Consistently [25], the pair distribution function reads

$$g_2(r) = \frac{1}{2\pi n(N-1)r} \left\langle \sum_i \sum_{j\neq i} \delta(r - r_{ij}(t)) \right\rangle_t \tag{4}$$

where n is the system density, and N the number of particles of the ensemble.

In accordance with Ref. [26], in a system where periodic boundary conditions are imposed, the estimator of the superfluid fraction can be defined as

$$f_S = \frac{m}{\hbar^2 \beta N} \langle \mathbf{w}^2 \rangle, \tag{5}$$

where $\beta = 1/k_B T$. The quantity $\mathbf{w} = (w_x, w_y)$ is the winding number estimator [26], defined as

$$\mathbf{w} = \sum_i \left(\mathbf{r}_i(t+1) - \mathbf{r}_i(t)\right). \tag{6}$$

We present data considering up to $N = 250$ particles and about 650 sites in order to exclude any finite-size effects. Even if the algorithm works at finite temperature, an accurate extrapolation of the ground state limit (i.e. $T \to 0$) may be reached as well. As a general rule, this limit is approached when the structural and energetic properties of the system remain constant within the statistical error of the simulation.

The phase diagram of the Hamiltonian (1) with $u_0 = 0$ has been intensively investigated over the last few years. At present, there is a general consensus that this phase diagram only presents a melting quantum phase transition from a triangular crystal to a homogeneous superfluid [17,18,27]. The crystal-superfluid quantum phase transition results seem to be easily controlled by adjusting the dimensionless parameters $r_\mathrm{d} = Dm/a\hbar^2$, a being the averaged interparticle distance of the purely continuous system. Büchler et al. have identified the transition at $r_\mathrm{d}^\mathrm{QM} = 18(4)$ [18]. Nevertheless, some aspects related to the transition order continue to be controversial. In particular, as discussed by Spivak and Kivelson [28], at the interface between the two phases, the system should feature a microemulsion phase. Using a variational quantum Monte Carlo [29], Moroni and Boninsegni have recently pointed out that "for all practical purposes" [17], the transition results of the first order, with a coexisting phase (microemulsion) mainly inaccessible for any possible experiment.

Differently from the case just discussed, the limit $u_0 \to \infty$ presents a more complex but also more interesting phase diagram. Here, between a superfluid and a crystal phase, Pollet et al. [13] identified a supersolid phase as well as a microemulsion as proposed in Ref. [28]. The authors found that for a commensurate filling factor $n = 1/3$ (n typically being the ratio between simulated particles and lattice size), the system displayed diagonal and off-diagonal long-range order concurrently.

In order to observe a supersolid phase, in this study, we were interested in analysing the unexplored limit of finite u_0, considering again the filling values $n = 1/3$ (commensurate filling) and $n \gtrsim 1/3$ (noncommensurate filling). The noncommensurate filling case was studied by introducing an interstitials density ranging from 0.02 to 0.04. In addition, we focused our attention on the limit $r_\mathrm{d} \lesssim r_\mathrm{d}^\mathrm{QM}$, in other words far from a free-space triangular lattice phase.

3 Results

3.1 Ground-State Properties

Figure 1 depicts snapshots of the projection of world lines onto the xy-plane for $n = 1/3$ (Fig. 1a), with a density of defects (interstitials) equal to 0.036 (Fig. 1b). The dipole–dipole interaction is $d = 15$ (i.e. $r_\mathrm{d} \approx 5$), while the lattice depth corresponds to $u_0 = 8$. The representation in Fig. 1 provides a functional way to sketch out the probability distribution of the many-body system in real space [20]. Below a superfluid transition temperature, the overlap of paths entails exchanges among bosons and superfluidity too.

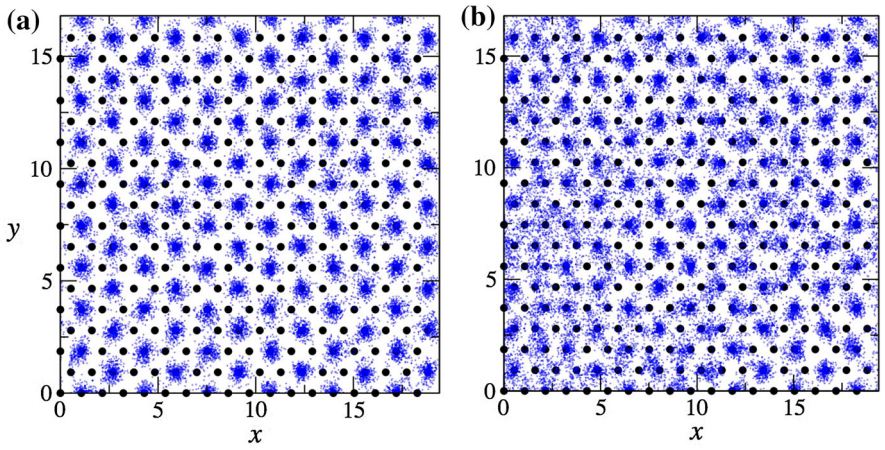

Fig. 1 Example of configuration snapshots, in other words particle world lines projection on an xy-plane, for a system of dipolar bosons confined in a two-dimensional optical lattice with Eq. (2). The *dots* represent the 325 sites, in other words the potential minimum. The interaction is $d = 15$ and the lattice depth is $u_0 = 8$. **a** $N = 108$ (no defects), and **b** $N = 120$ (density defect 0.036) (Colour figure online)

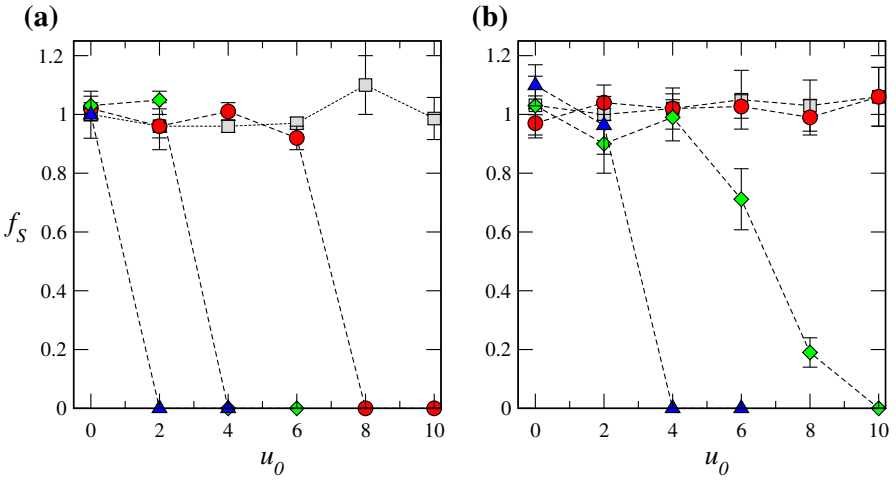

Fig. 2 Superfluid fraction versus lattice depth considering a system without defects (**a**) and introducing a defect density equal to 0.036. $r_{\mathrm{d}} = 1.67$ (*square*), 3.34 (*circle*), 5 (*diamond*) and 6.67 (*triangle*) (Colour figure online)

We observe in Fig. 1a that particle paths are completely confined around the local minima of the lattice potential (2), showing a stripe crystal ground state configuration. The situation changes if one introduces defects. Figure 1b depicts a configuration, whereby a localised path occurs with delocalised ones. This coexistence implies the presence of a supersolid phase.

Figure 2 shows the superfluid fraction f_{S} versus u_0, considering the different values of r_{d}, again for a commensurate (Fig. 2a) and an incommensurate (Fig. 2b) sample,

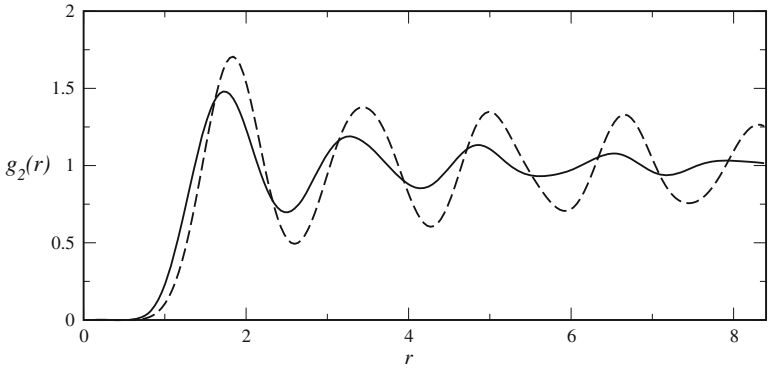

Fig. 3 Pair distribution function $g_2(r)$ for a crystal phase (*dashed line*) and a supersolid phase (*continuous line*), using the same set of parameters as in Fig. 1

respectively. Analysing Fig. 2a, we see that only for $r_d = 1.67$, the dipolar system persists in being superfluid ($f_S = 1$) over all the u_0 considered. However, by increasing r_d, we obtain a simple drop of the superfluid estimator from one (homogeneous superfluid) to zero (crystal) when the lattice depth turns deeper. Such behaviour signalises a simple superfluid-to-insulating-crystal quantum phase transition. The snapshot configuration in Fig. 1a is a representative example that shows how the lattice is forcing a crystal phase onto the system. In fact, for $u_0 = 0$, we have observed a superfluid phase for all the r_d considered.

Figure 2b shows simulations introducing defects, again for different r_d. Here for $r_d = 3.34$ and $u_0 \leq 10$, we notice that the presence of defects seems to remove only the transition, leaving the superfluid phase unchanged. Moreover, for interaction strengths $r_d = 1.67$ and 6.67, f_S does not show any fundamental changing with respect to the commensurate case. Yet, for $r_d = 5$ and $5 < u_0 < 9$, the ground-state superfluidity leads to a *nonhomogeneous* superfluid behaviour, characterised by $0 < f_S < 1$ [30]. This set of parameters allows the system to move into a supersolid phase, as shown in Fig. 1b.

Figure 3 reports the pair distribution function, introduced in equation (4). Such a function provides more qualitative information on a liquid or crystal phase. The figure still compares a commensurate (dashed line) and an incommensurate (continuous line) filling value, respectively. In either case, the system perfectly mimics the lattice periodicity, with the first maximum representing the averaged interparticle distance for a stripe crystal. Regarding the supersolid phase (continuous line), $g_2(r)$ still presents a robust modulation that becomes smoother at large distances due to a strong particle delocalisation throughout the lattice.

3.2 Finite Temperature Properties

Now we discuss the temperature effects on the supersolid phase observed in Figs. 1b and 2b. As one would expect, the stability of the condensate at finite temperature is a key feature for supporting realistic experiments. In order to clarify the behaviour in

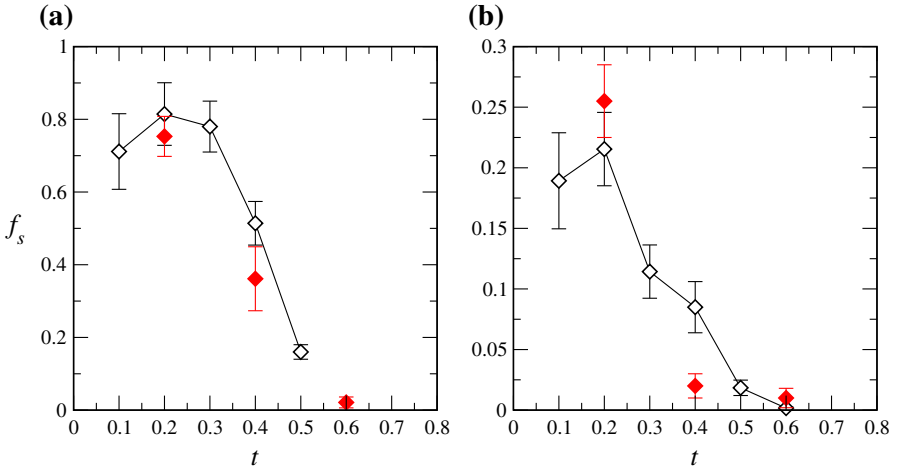

Fig. 4 Superfluid fraction versus the reduced temperature t with a defect density equal to 0.036 considering $u_0 = 6$ (**a**) and $u_0 = 8$ (**b**). $N = 120$ (*open diamond*) and 212 (*full diamond*) (Colour figure online)

temperature, Fig. 4 depicts the superfluid fraction as a function of temperature, for $u_0 = 6$ (Fig. 4a) and 8 (Fig. 4b), respectively. In accordance with Fig. 2b, we take into account a dipole strength ($r_d = 5$) that furnishes a nonhomogeneous superfluidity for $t \to 0$. We defined a reduced temperature $t \equiv k_B T/(\hbar^2 n/m)$, $\hbar^2 n/m$ being the kinetic energy at the mean interparticle distance.

Considering first $u_0 = 6$ for an ensemble of $N = 120$ dipoles, one sees that f_S remains constant ($f_S \sim 0.75$) up to $t \lesssim 0.4$, revealing a critical behaviour at finite t (temperature phase transition). This, therefore, appears as entirely consistent with the Berezinsky–Kosterlitz–Thoules (BKT) theory for a two-dimensional system with a continuous symmetry [31]. It is well known that for a homogeneous gas of bosons, the transition temperature can be estimated at $T_{BKT} = 2\pi\hbar^2 n/mk_B$. Figure 4b shows that this approximation yields a BKT regime for $t \lesssim 0.85$. The lowering of the BKT regime in temperature is strictly connected with the interaction strength showed in Fig. 4, consistent with the results discussed in Ref. [32]. Figure 2b shows a similar physics for $t \lesssim 0.3$ but with a lower superfluid fraction in the ground state ($f_S \sim 0.22$). We observe that in the supersolid region, u_0 appears to influence t_{BKT} only mildly. This, actually, is an interesting feature of dipolar bosons in an optical lattice. For $u_0 > 8$, we do not observe any superfluidity (and consequently any t_{BKT}), leading to the onset of a crystal phase. These results seem to be consistent with a first-order phase transition. It is worthwhile stressing that a crystal-to-supersolid first-order phase transition has been observed also for ultra-cold soft-core bosons [33,34] and for dipolar bosons in triangular lattices [35] as well.

Finally, in order to exclude finite-size effects, Fig. 4 compares two different system sizes, $N = 120$ (open diamond) and $N = 212$ (full diamond). It clearly appears that superfluidity at finite temperature does not change within the statistical errors for both sizes.

4 Conclusions

In this study, we considered a two-dimensional dipolar bosonic gas in the presence of a weak triangular optical lattice. The results were obtained using an exact quantum Monte Carlo that implements the worm algorithm in continuous space. Different from previous studies, we investigated a Hamiltonian (1) modifying the depth of the optical lattice (2) and the strength of the dipole–dipole interactions. Regarding a commensurate filling, we observed that the presence of a periodic potential did not change the phase diagram of the system for $u_0 = 0$, in other words where the quantum gas simply shows a crystal-to-superfluid quantum phase transition. In contrast, the introduction of defects into the system was found to allow a clear defect-induced supersolidity. We also verified that this phase remained thoroughly solid even at finite temperature. Finally, the supersolid mechanism here discussed fully agrees with the original definition of supersolid phase given by Andreev and Lifshitz [19]. In this limit of density, our results therefore proved that the experimental realisation of this long-sought quantum phase can also be made using quantum dipolar gases in optical lattices.

Acknowledgments The author thanks G. Pupillo and T. Macrì for enlightening discussions.

References

1. C. Becker, P. Soltan-Panahi, J. Kronjäger, S. Dörscher, K. Bongs, K. Sengstock, New J. Phys. **12**(6), 065025 (2010)
2. J. Sebby-Strabley, M. Anderlini, P.S. Jessen, J.V. Porto, Phys. Rev. A **73**, 033605 (2006)
3. P. Schauß, J. Zeiher, T. Fukuhara, S. Hild, M. Cheneau, T. Macrì, T. Pohl, I. Bloch, C. Gross, Science **347**(6229), 1455 (2015)
4. B. Yan, S.A. Moses, B. Gadway, J.P. Covey, K.R.A. Hazzard, A.M. Rey, D.S. Jin, J. Ye, Nature **501**(7468), 521 (2013)
5. S. Baier, M.J. Mark, D. Petter, K. Aikawa, L. Chomaz, Z. Cai, M. Baranov, P. Zoller, F. Ferlaino, arXiv:1507.03500v1
6. M.A. Baranov, Phys. Rep. **464**(3), 71 (2008)
7. T. Lahaye, C. Menotti, L. Santos, M. Lewenstein, T. Pfau, Rep. Prog. Phys. **72**(12), 126401 (2009)
8. M. Boninsegni, N.V. Prokof'ev, Rev. Mod. Phys. **84**, 759 (2012)
9. F. Cinti, T. Macrì, W. Lechner, G. Pupillo, T. Pohl, Nat. Commun. **5** (2014)
10. W. Lechner, D. Polster, G. Maret, P. Keim, C. Dellago, Phys. Rev. E **88**, 060402 (2013)
11. I. Danshita, D. Yamamoto, Phys. Rev. A **82**, 013645 (2010)
12. M. Boninsegni, N. Prokof'ev, Phys. Rev. Lett. **95**, 237204 (2005)
13. L. Pollet, J.D. Picon, H.P. Büchler, M. Troyer, Phys. Rev. Lett. **104**, 125302 (2010)
14. U. Bissbort, F. Deuretzbacher, W. Hofstetter, Phys. Rev. A **86**, 023617 (2012)
15. H.P. Büchler, Phys. Rev. Lett. **104**, 090402 (2010)
16. W. Lechner, F. Cinti, G. Pupillo, Phys. Rev. A **92**, 053625 (2015)
17. S. Moroni, M. Boninsegni, Phys. Rev. Lett. **113**, 240407 (2014)
18. H.P. Büchler, E. Demler, M. Lukin, A. Micheli, N. Prokof'ev, G. Pupillo, P. Zoller, Phys. Rev. Lett. **98**, 060404 (2007)
19. A.F. Andreev, I.M. Lifshitz, Sov. Phys. Jetp USSR **29**(6), 1107 (1969)
20. D.M. Ceperley, Rev. Mod. Phys. **67**, 279 (1995)
21. M. Boninsegni, N. Prokof'ev, B. Svistunov, Phys. Rev. Lett. **96**, 070601 (2006)
22. L. Pollet, Rep. Prog. Phys. **75**(9), 094501 (2012)
23. M. Boninsegni, N.V. Prokof'ev, B.V. Svistunov, Phys. Rev. E **74**(3), 036701 (2006)
24. P. Jain, F. Cinti, M. Boninsegni, Phys. Rev. B **84**, 014534 (2011)
25. M. Plischke, B. Bergersen, Equilibrium Statistical Physics (World Scientific, 2006)
26. E.L. Pollock, D.M. Ceperley, Phys. Rev. B **36**, 8343 (1987)

27. G.E. Astrakharchik, J. Boronat, I.L. Kurbakov, Y.E. Lozovik, Phys. Rev. Lett. **98**(6), 060405 (2007)
28. B. Spivak, S.A. Kivelson, Phys. Rev. B **70**, 155114 (2004)
29. A. Sarsa, K.E. Schmidt, W.R. Magro, J. Chem. Phys. **113**(4), 1366 (2000)
30. A.J. Leggett, Phys. Rev. Lett. **25**, 1543 (1970)
31. P. Chaikin, T. Lubensky, T. Witten, *Principles of condensed matter physics* (Cambridge University Press, Cambridge, 2000)
32. A. Filinov, N.V. Prokof'ev, M. Bonitz, Phys. Rev. Lett. **105**, 070401 (2010)
33. T. Macrì, F. Maucher, F. Cinti, T. Pohl, Phys. Rev. A **87**, 061602 (2013)
34. F. Cinti, M. Boninsegni, T. Pohl, New J. Phys. **16**(3), 033038 (2014)
35. D. Yamamoto, I. Danshita, C.A.R. Sá de Melo, Phys. Rev. A **85**, 021601 (2012)